CHAPTER 3 ELECTRON COLLISION WITH ANALOGOUS OF DNA/RNA NUCLEOBASES

"This chapter presents the results for electron collision processes with analogous bio-molecules of DNA/RNA, 3-hydroxy-tetrahydrofuran and α-tetrahydrofurfuryl alcohol, which exhibit structural and functional group similarities to backbone of DNA/RNA. The SCOP formalism is employed to compute total elastic (Q_{el}) and inelastic (Q_{inel}) CSs. Total ionization (Q_{ion}) and summed total excitation ($\sum Q_{exc}$) cross sections are obtained using the CSP-ic formalism. These findings cover a broad energy range10 eV to 5 KeV, biomolecular damage caused by secondary electrons via primary ionization may be predicted using input parameters. We have found a relationship between the number of valence electrons (Nv), ionization energy (IE), and Q_{ion}^{max} and molecule polarizability (α)".

3.1 Introduction

"High Resolution Electron Energy Loss Spectroscopy (HREELS)" is a most effective technique [1,2] to measure and study absolute cross sections for Low Energy Electrons (LEEs) interact with bio-molecules [3,4].

These CSs are used for dose calculations in radiotherapy for cancer treatment. Radiotherapy is very effective and essential tool in cancer treatment [5]. LEEs are important because of their significance in a wide range of other fields involving "high energy ionization radiation (HEIR)" [6]. These include Planetary Science [7], astrochemistry [8], plasma science [9], extreme UV photon nanolithography, bio-medical imaging, and radioprotection [10], dosimetry for irradiation in space [11]. When "high energy ionization radiation" (i.e. X-rays, β-rays, ϒ-rays, and others) interact with bio molecules including DNA and its constituents and deposit their energy via biological medium several ions, radicals, secondary electrons (~10^4 electrons per MeV) are produced. By inelastic processes low energy secondary electrons interact with bio-molecules via biological medium. LEEs have the ability to cause cluster DNA/RNA damage through single-strand (SSBs) and double strand (DSBs) breaks, base dilation etc.

To understand and predict these damages, Monte Carlo codes [12] are used in nanoscopic scales which requires a vast number of variables relating to interaction probabilities. Moreover, It is challenging to comprehend electron interactions with DNA at low to intermediate energies because of a scarcity of the data and also its ultrafast reaction (10^{-18} to 10^{-15} sec). It is very useful to study the constituents of DNA and analogues of deoxyribose sugar molecules in the gas phase including 3-hydroxytetrahydrofuran (3H-THF) and α-tetrahydrofurfuryl alcohol (THFA) molecules.

Deoxyribose is primarily existing in the pyranose form, a six-membered ring. To specifically investigate the stability of the furanose ring under electron interactions, several analogues, tetrahydrofuran (THF) [13], 3-hydroxytetrahydrofuran (3H-THF), and α-tetrahydrofurfuryl alcohol (THFA) were used as corresponding targets.

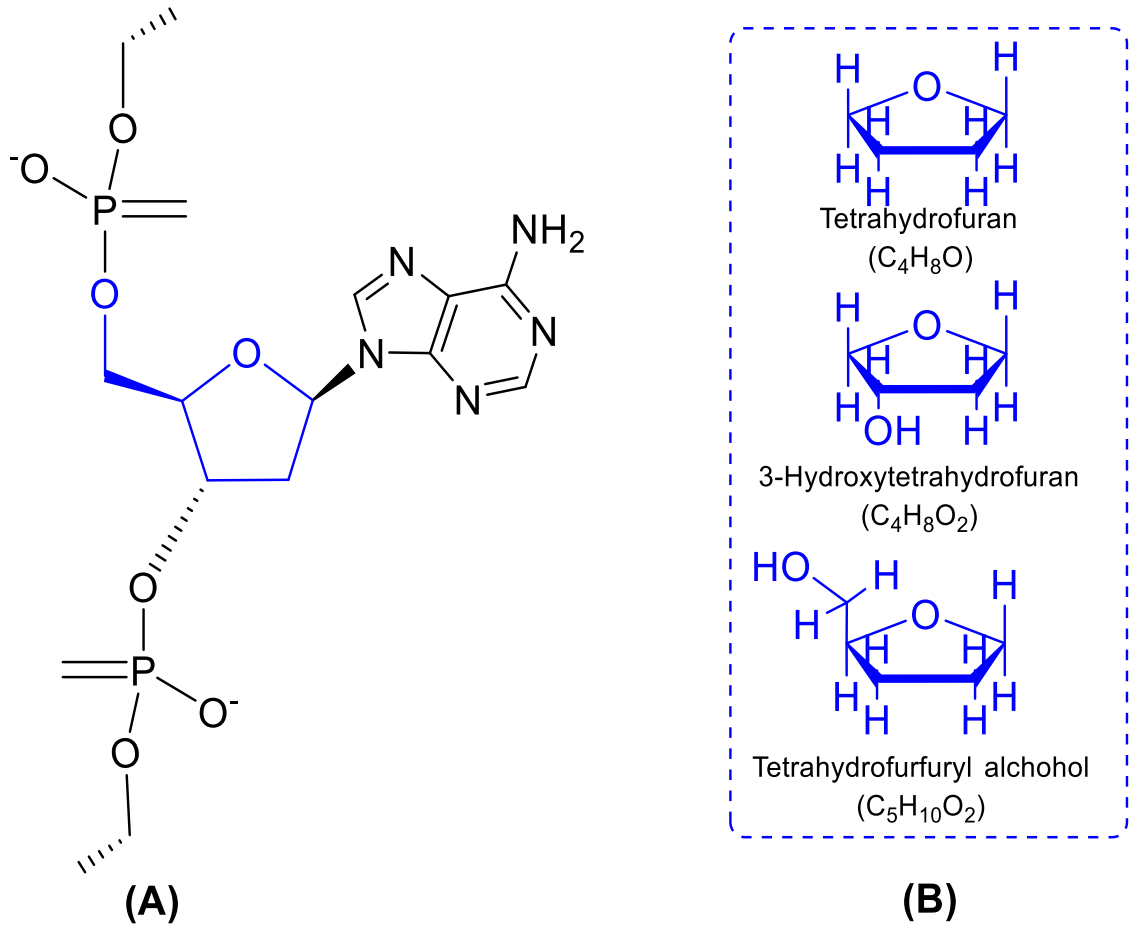

Figure 3.1 Schematic diagram of single-stranded DNA with the molecules of biological relevance

Primary objectives of this study, offers trustworthy probabilities for various molecular processes through estimation of inelastic, ionization, elastic, electronic excitation, and total CSs for electron interactions with analogous molecule of sugar backbone of 2-deoxyribose such as THFA and 3H-THF. The schematic of present targets is shown in Figure 3.1.

3.2 3-Hydroxytetrahydrofuran ($C_4H_8O_2$)

Here, we present and discuss the results of electron collision from the 3-Hydroxytetrahydrofuran. This molecule was investigated using the SCOP and CSP-ic formalism to compute variety of CSs viz. Q_T, Q_{el}, Q_{inel}, Q_{ion} and ΣQ_{exc}. 3-Hydroxytetrahydrofuran is a heterocyclic ether structurally similar to THF. As previously noted, molecules like tetrahydrofuran and 3-hydroxytetrahydrofuran are of particular interest to the scientific community due to their role as sugar rings within the backbone structure of nucleic acids. Consequently, they can be considered fundamental building blocks of life (see Figure 3.1).

3.2.1 Literature study and target properties

All of these investigations are addressed in table 3.1. The following is a review of earlier research on $C_4H_8O_2$.

Table 3.1 Literature survey of e- $C_4H_8O_2$

Mol.	Qty.	Methods	E_i (eV)	Ref.
$C_4H_8O_2$	Q_{ion}	Binary-Encounter-Bethe (BEB) [Th.]	IE to 4000	[14]
	Q_{inel}	IAM-SCAR [Th.]	5-10000	[15]
	Q_{el}	Phase shift analysis approach [Ex; ±20%]	6,10,15,20	[16]
		IAM-SCAR [Th.]	5-10000	[15]
	Q_T	IAM-SCAR [Th.]	5-10000	[15]

In the Table 3.2 Schematic and target properties of $C_4H_8O_2$ are given.

Table 3.2 Schematic and properties of $C_4H_8O_2$

Schematic	IP (eV)	Polarizability (Å^3)
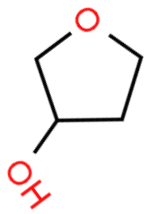	9.51	8.60

Table 3.3 Cross-sections data ($Å^2$) for $C_5H_{10}O_2$

E_i (eV)	Q_{ion}	Q_{el}	Q_T
10	0.00	92.61	92.66
20	4.67	62.11	72.56
30	10.36	44.89	63.36
40	13.85	35.08	57.30
50	15.81	28.94	52.62
60	16.84	24.93	48.94
70	17.29	21.83	45.56
80	17.39	19.71	42.86
90	17.30	17.88	40.31
100	17.05	16.64	38.29
200	13.65	10.10	25.60
300	11.17	7.28	19.44
400	9.46	5.78	15.84
500	8.22	4.77	13.40
1000	5.03	2.62	7.76
2000	2.88	1.43	4.34
3000	2.02	1.01	3.04
4000	1.55	0.79	2.35

5000	1.27	0.68	1.95

3.2.2 Results

For 3-Hydroxytetrahydrofuran ($C_4H_8O_2$), we present the CSs results for impact energy starting from threshold to 5 KeV. We separated our investigation into two categories and presented them as follows, taking into account the available comparisons:

(i) Inelastic cross sections:

Here, graphical findings from Q_{inel}, Q_{ion} and ΣQ_{exc} have been reported. Q_{ion} ionization CSs are computed using the CSP-ic .

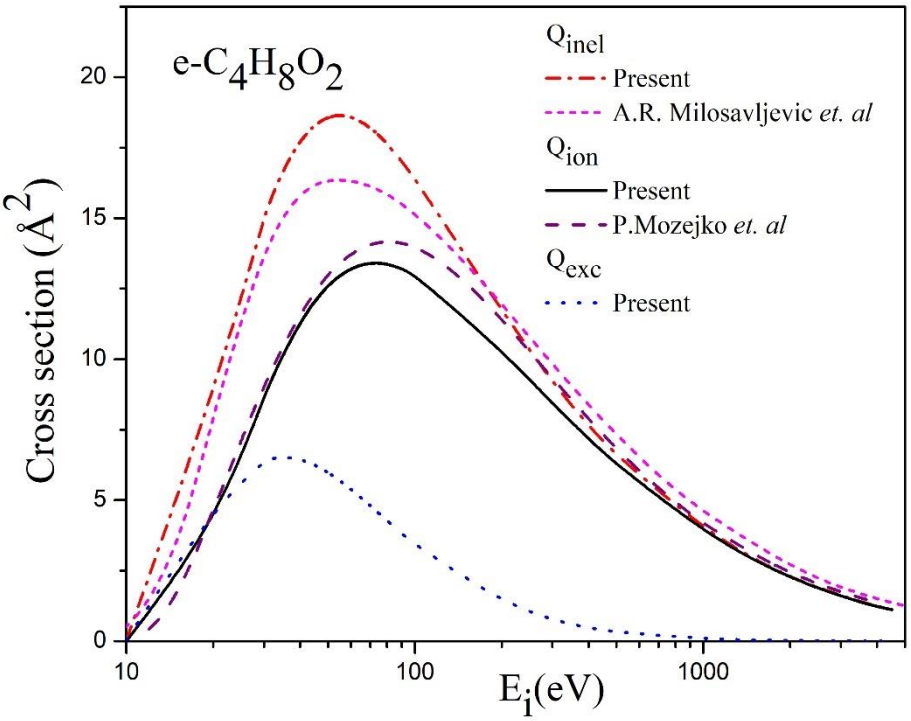

Figure 3.2 Q_{inel}, Q_{ion} and ΣQ_{exc} for e- $C_4H_8O_2$ collision

Q_{inel}: dash dot -Present, short dash- [15], Q_{ion} : solid - Present, dash- [14], Q_{exc}: dot - Present.

In Figure 3.2, we illustrate present Q_{inel}, Q_{ion}, and $\sum Q_{exc}$ for e-$C_4H_8O_2$ molecule. The cross-sections data are tabulated in Table 3.3. Here, we compare present Q_{inel} with available

theoretical data [15]. They have used IAM-SCAR method for 5 eV to 10 Kev. It's seen that present inelastic CSs overestimate the result of IAM-SCAR in the peak region. However, they [15] show good accord at lower energies and beyond 200 eV. We show the Q_{ion} with the same energy range and compare with [14]. It gives good agreement with the BEB method proposed by [14]. There are no direct results available to compare excitation CSs ($\sum Q_{exc}$).

(ii) Total and elastic CSs:

The graphical output representation of Q_T and Q_{el} is included in this category.

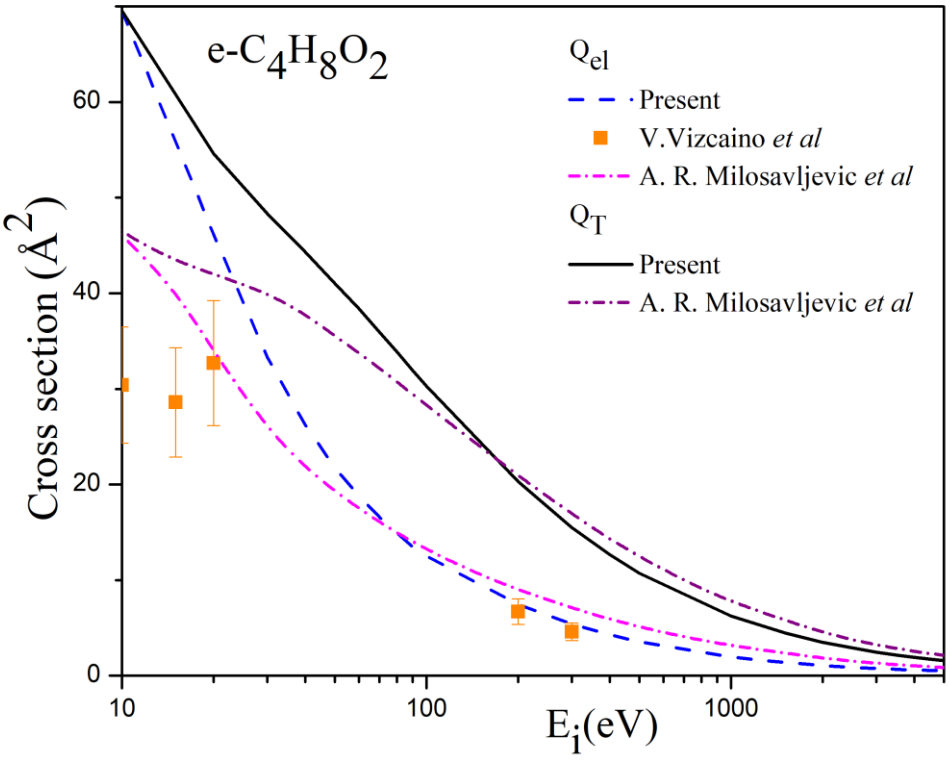

Figure 3.3 Q_T and Q_{el} for e- $C_4H_8O_2$ collision

Q_{el}: Short dot dash - Present, short dot dash- [15], Full Square- (Exp.) [16], Q_T: solid - Present, short dot dash-[15]

Our absolute results of elastic CSs (Q_{el}) and total CSs(Q_T) for $C_4H_8O_2$ scattering are shown in figure 3.3. Present Q_{el} is compared with experimental [16] and theoretical [15] results. An integral elastic CSs have been experimentally measured by [16] using a phase-shift analysis

approach within certain energy 10 eV,15 eV, and 20 eV. For energy threshold to 100 eV, present Q_{el} is overestimated with available experimental data [16] and for intermediate energy (200 eV & 300 eV), they show good agreement with the available experimental data.

Present, Q_{el} and Q_T are matching well with theoretical data of [15], they were obtained by the "Screen Corrected Additivity Rule (SCAR)" method and followed the same trend for intermediate energy to 5 KeV.

3.3 *α*-Tetrahydrofurfuryl alcohol ($C_5H_{10}O_2$)

In this section, Literature survey, target properties and various cross-sectional studies have been discussed for the electron scattering of THFA ($C_5H_{10}O_2$) molecule.

3.3.1 Prior work and target properties

We discuss all these investigations in table 3.4. Let us review the prior work on the $C_4H_8O_2$ as follows:

Table 3.4 Prior work of e-$C_5H_{10}O_2$

Mol.	Qty.	Methods	E_i (eV)	Ref.
$C_5H_{10}O_2$	Q_{ion}	Binary-Encounter-Bethe [Th.]	IE to 4000	[14]
		IAM-SCAR [Th.]	1-1000	[17]
		Absolute Total Ionization cross section cell [Ex; ±4%]	10-285	[18]
		Through swarm data [Th.]	10-1000	[19]
	Q_{inel}	IAM-SCAR [Th.]	5-5000	[20]
		IAM-SCAR [Th.]	1-1000	[17]
	Q_{exc}	Electron monochromator [Ex.; ±30-45 %]	20-50	[17]
	Q_{el}	IAM [Th.]	50-2000	[14]
		IAM-SCAR [Th.]	5-5000	[20]
		IAM-SCAR [Th.]	1-1000	[17]
		Through swarm data [Th.]	10-1000	[19]
	Q_T	IAM & Binary-Encounter-Bethe [Th.]	IE-4000	[14]

		Linear transmission technique [Ex.]	1-370	[21]
		IAM-SCAR [Th.]	5-5000	[20]
		IAM-SCAR [Th.]	1-10000	[22]
		IAM-SCAR [Th.] and IAM-SCAR+R[Th.]	1-1000	[17]
		Through swarm data [Th.]	10-1000	[19]

Table 3.5 Schematic and Properties of $C_5H_{10}O_2$

Target	**IP (eV)**	**Polarizability ($Å^3$)**
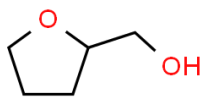	9.47	10.40

Table 3.6 Cross-sections data ($Å^2$) for $C_5H_{10}O_2$

E_i (eV)	**Q_{ion}**	**Q_{el}**	**Q_T**
10	0.00	53.37	53.43
20	3.68	34.44	47.81
30	8.41	24.88	47.40
40	11.50	19.82	46.23
50	13.34	16.72	44.36
60	14.40	14.70	42.33
70	14.99	13.13	40.16
80	15.27	12.02	38.20

90	15.36	11.05	36.27
100	15.30	10.26	34.48
200	12.96	6.07	22.88
300	10.90	4.35	17.36
400	9.41	3.41	14.14
500	8.29	2.79	11.98
1000	5.27	1.50	l7.02
2000	3.11	0.79	3.97
3000	2.22	0.56	2.80
4000	1.72	0.44	2.17
5000	1.41	0.20	1.62

3.3.2 Results

Here, we describe full set of CSs viz. Q_{inel}, Q_T, Q_{ion} , Q_{el} , and ΣQ_{exc} of electron impact with α-Tetrahydrofurfuryl alcohol ($C_5H_{10}O_2$) along with available comparison.

(i) Inelastic collision

A variety of CSs, which comes under the effects of inelastic are displayed in figure 3.4 and CSs data is provided in table 3.6.

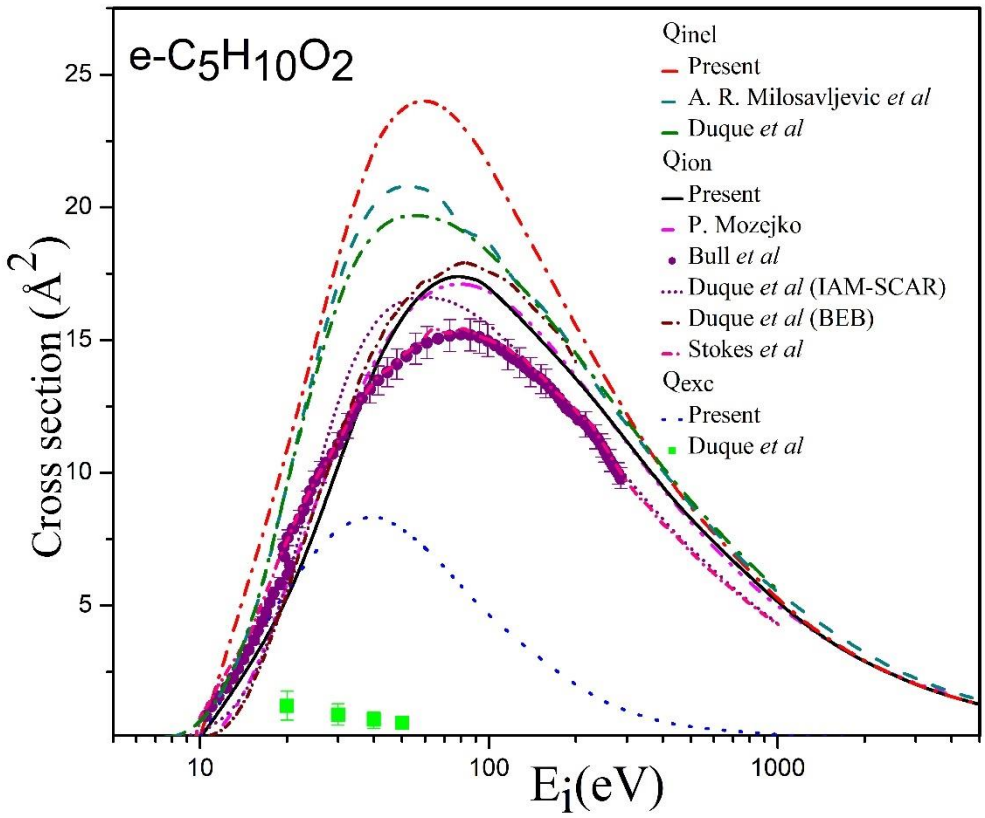

Figure 3.4 Q_{inel}, Q_{ion} and ΣQ_{exc} for e-$C_5H_{10}O_2$

Q_{inel}: dash dot -Present, dash - [20], dash dot - [17] -Q_{ion}: Red Solid - Present, dash dot dot - [14], Dark pink solid [19], short dash dot (BEB) and short dot (IAM-SCAR) - [17], Circle-[18], Q_{exc}: dot - Present, square-[17]

In Figure 3.4 we have presented Q_{inel}, Q_{ion}, and Q_{exc} for e-$C_5H_{10}O_2$ along with theoretical and experimental comparison. The upper curve with a dash dot called present Q_{inel} is shown in Figure 3.4. Present Q_{inel} data are compared available theoretical data of [17] and [20] [Excitation + Neutral dissociation+ Ionization] and we found good agreement with IAM-SCAR obtained by [17] and [20] at an energy between 200-5 keV. Present Q_{ion} is in reasonably good accord with semi-classical (BEB) formalism by [14] and [17]. Besides, they also reported ionization CSs predicted using the IAM-SCAR model by [17] which is quite lower than our present Q_{ion}. Experimentally, Q_{ion} data were measured using the absolute total ionization CSs cell by [18] (under ±4% uncertainty).

Figure 3.4 compares present electronics excitation CSs for e-THFA with experimental integral CSs (ICS) data of [17]. This author[17] identified five Rydberg electronic-state bands reported Band 1+2, Band 3, and Band 4+5 with an energy range of 20, 30, 40, and 50 eV, which monotonically decreased with increased energy. Here, we compare our present $\sum Q_{exc}$ with the sum of all Rydberg electronic-state within stated uncertainty of 24 to 34 percent. It underestimates with our present results.

(ii) Total and elastic collision

Here, we describe the present findings of Q_T and Q_{el} along with available theoretical and experimental data.

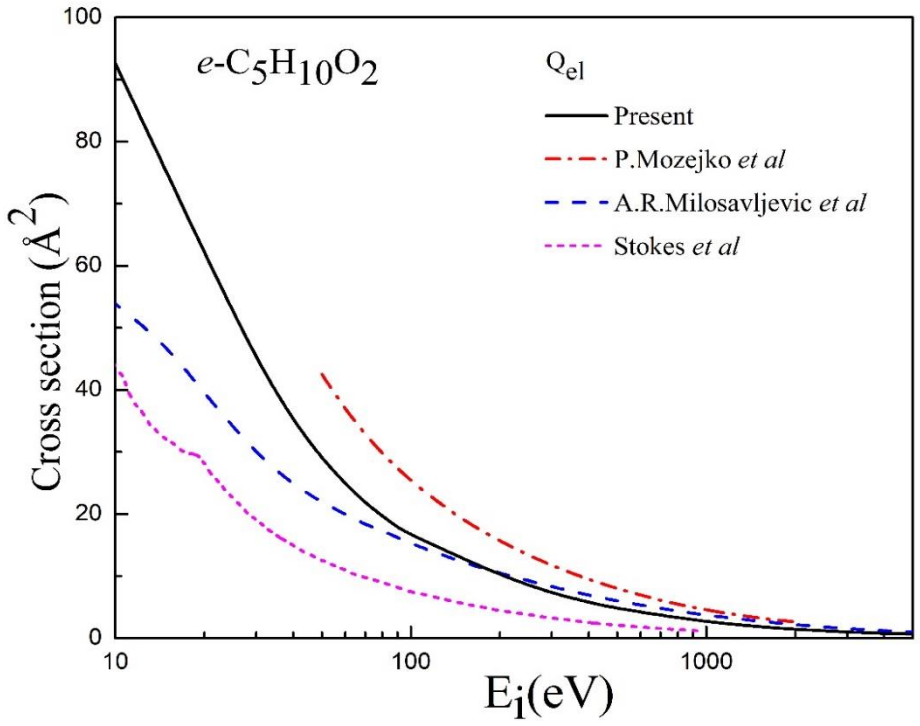

Figure 3.5 Q_{el} for e-$C_5H_{10}O_2$

Q_{el}: solid -Present, dash dot - [14], dash - [15], short dash - [19]

Our elastic CSs values for e-THFA are reported in Table 3.6 and the graphically plotted in Figure 3.5 with the available theoretical data of [14,15] and [19]. At 10-90 eV, present data overestimates the data obtained through IAM-SCAR method [15] and Neural network-based swarm data [19]. Present data gives good accord with IAM-SCAR [15] beyond 100 eV and data of [19] beyond 500 eV.

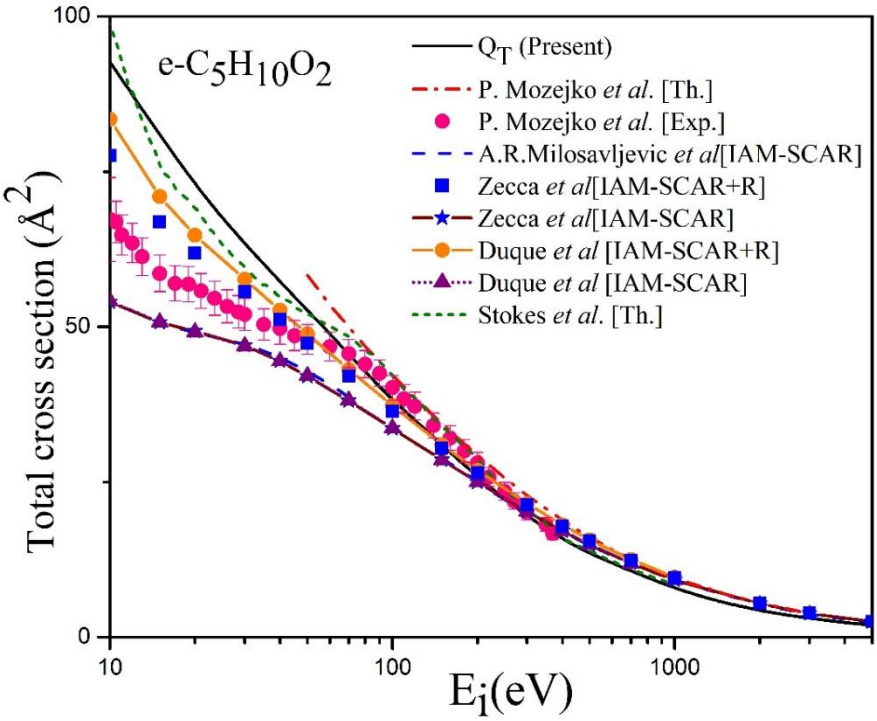

Figure 3.6 Q_T for e-$C_5H_{10}O_2$

Q_T: Solid -Present, dash- [15], dash dot - [14], circle- [21], Square- [22] , Short dash - [19], circle + line [17] (IAM-SCAR+R), short dash + triangle -IAM-SCAR [40]

Present total CSs data for e-THFA are shown in Figure 3.6. The experimental result of [21] and theoretical results of [14,15,17,19,22] are in good matching with the present results beyond ~70-80 eV. Below ~70 eV, our results overestimate the experimental results of [21] within ~5-6% uncertainty. They also reproduced the TCS data by summing the elastic and ionization CSs, earlier calculated [14] using IAM and BEB methods respectively. It can be seen from the figure 3.6 that the present data underestimate this reproduced data. This deviation is seen due to the fact that the theory which was used by them is not as reliable as to produce the data at lower energy [14]. Present Q_T, overestimate the available theoretical data obtain through IAM-SCAR method [20,40], which includes all elastic and inelastic effect except DEA, rotational, vibrational excitation. The TCS computed by using IAM-SCAR+R. [22] is in good accord, which includes rotational excitation but except DEA and vibrational excitation. Moreover, TCS data of [17] acquired by IAMSCAR+R method gives reasonably good matches with the shape and absolute CSs with present Q_T data. The grand TCS data of [19] is in good

agreement with present result. To compute grand TCS, authors first correct the forward-scattering effect in experimental data of [21], by enlarging the CSs magnitude at lower energies. At intermediate to high energy, they chose theoretical TCS data of [17] with their proposed DEA and Vibrational excitation cross sections. Then, they scaled experimental data of [21] to best fit this approximation.

3.4 Total ionization cross sections with available comparison

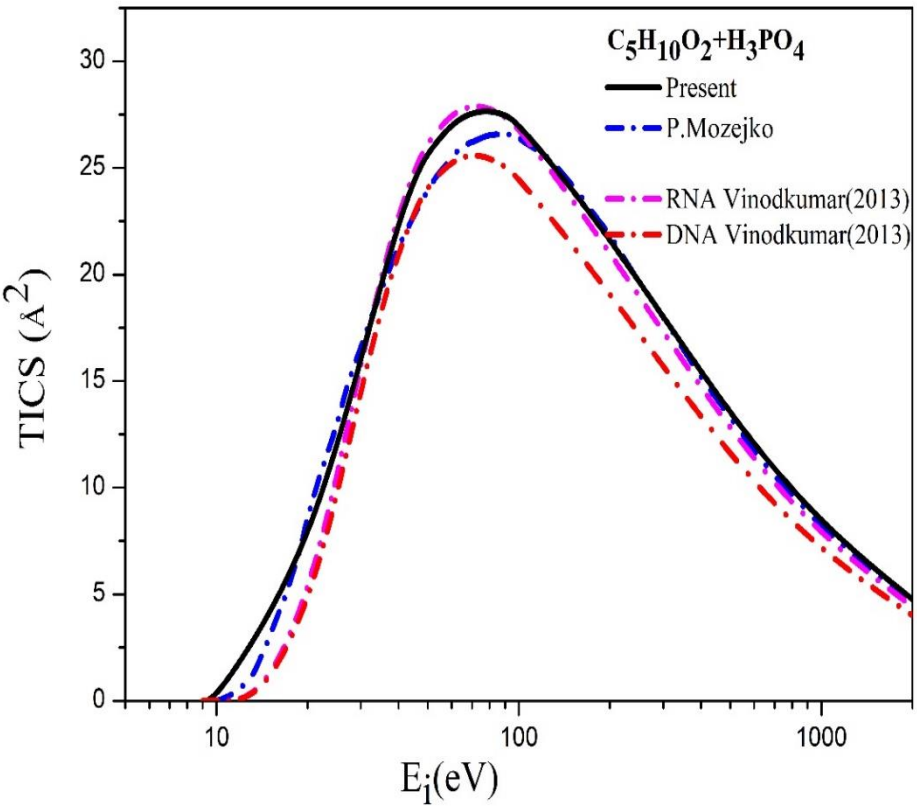

Figure 3.7 Total ionization CSs of $C_5H_{10}O_2$+H_3PO_4 along with DNA, RNA backbone

Previous studies have demonstrated that in certain cases and within specific approximations, electron induced ionization CSs for polyatomic molecules can be estimated based solely on fundamental atomic properties. Applying this approximation, we estimated ionization CSs for backbone of DNA/RNA by combining the present results for $C_5H_{10}O_2$ and that of H_3PO_4, taken from [24].

In Figure 3.7 the resulting values are compared with those of calculated by [24]. The combination of $C_5H_{10}O_2$ + H_3PO_4 [24] gives good accord with DNA and RNA backbone and [14].

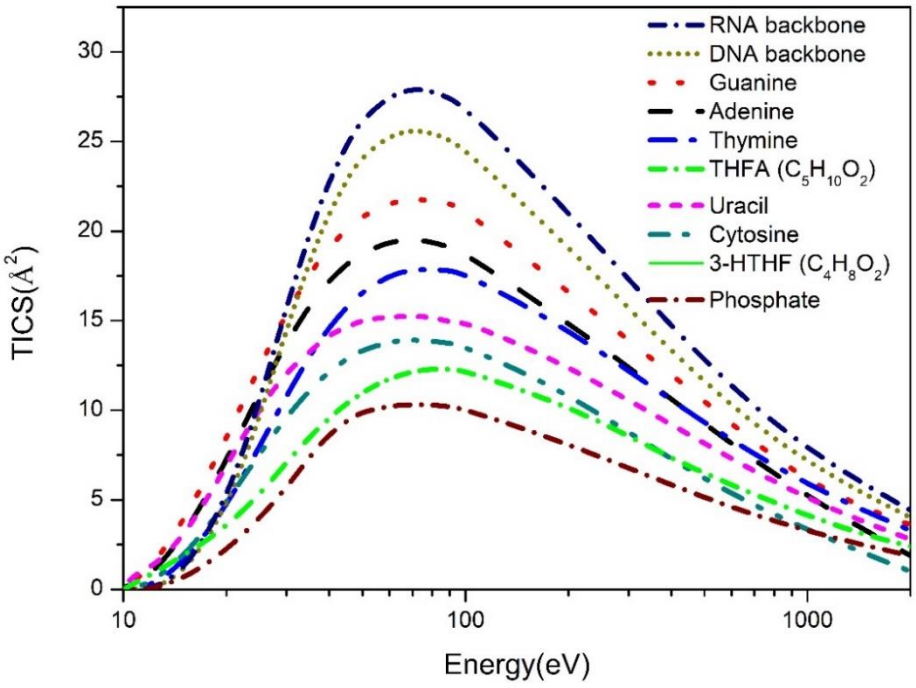

Figure 3.8 Comparison of the e-TICS for DNA/RNA constituents and present targets

RNA backbone [24], DNA backbone [24], Guanine [24], Adenine [24], Thymine [24], $C_5H_{10}O_2$ (THFA), Uracil [24], Cytosine [24], $C_4H_8O_2$ (3-HTHF), and phosphoric acid molecules.

Figure 3.8 compares total Q_{ion} data of DNA, RNA bases and phosphoric acid [24] with the present studied molecular targets 3-HTHF and THFA. In general, over the whole energy range examined (IE-2000 eV), the amplitude of the ionization CSs follows the pattern, which is similar to [14] and [25].

$$Q_{RNA} > Q_{DNA} > Q_{Guanine} > Q_{Adenine} > Q_{Thymine} > Q_{C5H10O2} > Q_{Uracil} > Q_{Cytosine} > Q_{C4H8O2} > Q_{Phosphoric\ acid}$$

When the number electrons of the molecule increase, the peak of the ionization CSs increases, which is clearly reflected in the Figure 3.8.

3.5 Correlation study and analysis of results

It is known that atomic and molecule properties like the ionization energy (IE), the intensity of the van der Waals contact, or the molecular volume are connected to the polarizability. The polarizability volume is proportional to the molecule's size as viewed by the incoming electron. Significant research of [26] on such correlations has been conducted by atomic and molecular systems. When no researchers provide a comparison, the correlation is a very useful characteristic for determining the reliability and consistency of the CSs data. If we know either peak Q_{ion}^{Max} or dipole polarizability (α), this correlation is useful to estimate any of them roughly.

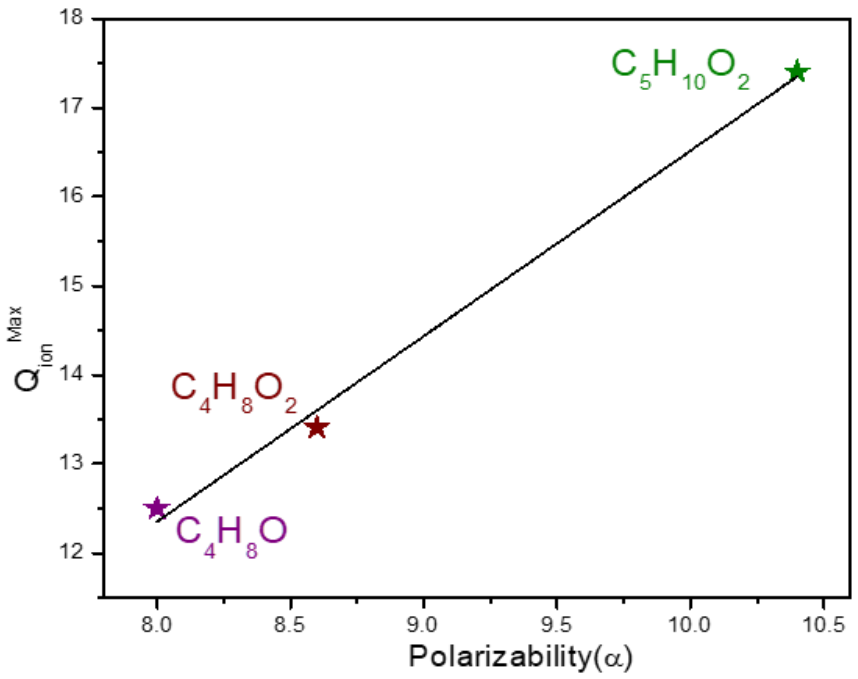

Figure 3.9 Correlation between Q_{ion}^{Max} and dipole polarizability (α)

For the sake of consistency of current studied molecules and tetrahydrofuran (THF), we took Q_{ion}^{Max} data from [27], presented in Table 3.7 to check linear correlation. In Figure 3.9, we can see this correlation between maximum Q_{ion} and dipole polarizability (α). The slight variation in the points can be attributed to uncertainties in the published polarizability values and differences in the group additivity rules applied for calculating the cross-section (CS) data of [28].

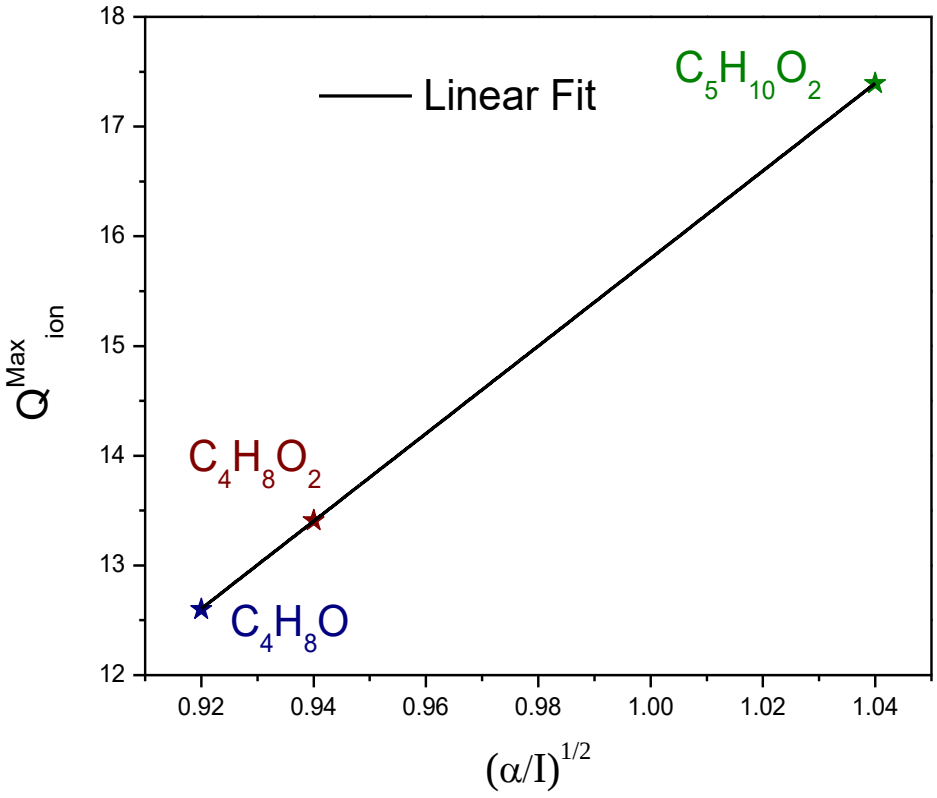

Figure 3.10 Correlation between Q_{ion}^{Max} and $\sqrt{\alpha/I}$

Additionally, figure 3.10 shows the relationship between square root of the ratio of polarizability and ionization potential $\sqrt{\alpha/I}$. This feature allows to predict polarizability of a particular molecular target for which polarizability is not available in literature. Although accuracy of this procedure can be limited as it has been observed only for a very narrow range of values $\sqrt{\alpha/I}$.

Table 3.7 Proparties of target molecules and computed data

Target	IP (eV)	α (Å³)	N_V	Energy at peak of ionization (eV)	Peak Q_{ion} (Å²)	Energy at peak of excitation (eV)	Peak $\sum Q_{exc}$ (Å²)
$C_4H_8O_2$	9.51	8.60	36	74	13.41	35	6.518
$C_5H_{10}O_2$	9.47	10.40	42	80	17.394	40	8.362
C_4H_8O [27]	9.38	8.00	30	76	12.50	---	---

Furthermore, we can see the scalability of total Q_{ion} is well proportional to number of valence electrons (N_V) of various target molecules at different electron impact energy range.

Table 3.8 Analytical relation for Q_{ion}^{Max}

	Linear fit	Linear fit passing through origin
Q_{ion}^{Max} as a function of α	Q=2.09(α)-4.30	Q=1.62(α)
Q_{ion}^{Max} as a function of $\sqrt{\alpha/I}$	Q=39.91($\sqrt{\alpha/I}$)-24.11	Q=14($\sqrt{\alpha/I}$)
Q_{ion}^{Max} as a function of N_V	Q=0.45(N_V)-1.51	Q=0.41(N_V)

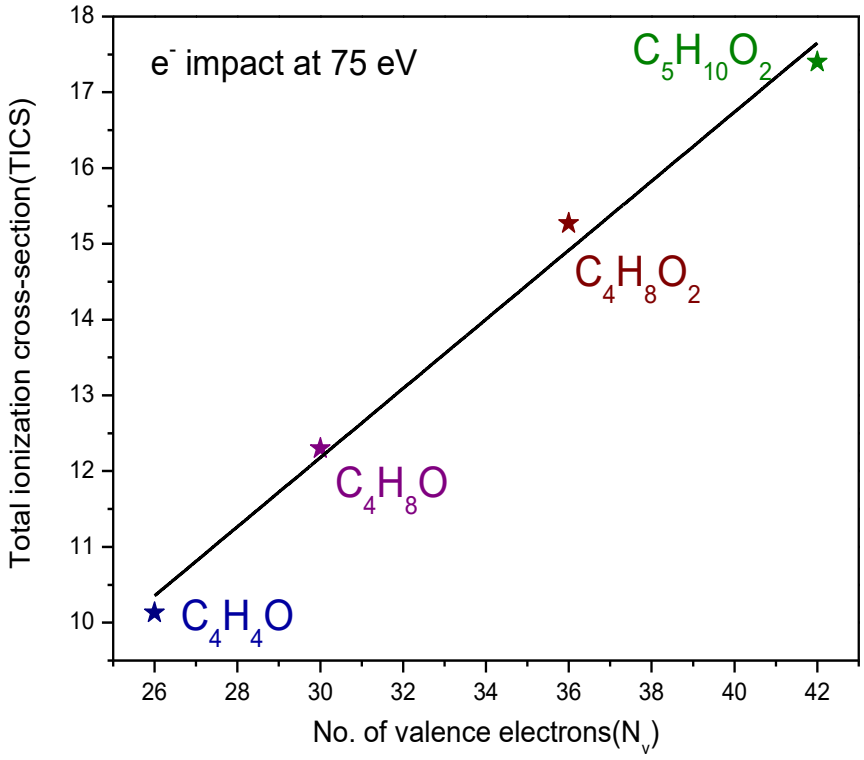

Figure 3.11 TICS plotted vs No. of valence electron (N_V) for various Molecular target obtained at 75 eV for electron impact.

In Figure 3.11 we show Q_{ion} vs number of valance electrons (N_V) at 75 eV. In Table 3.8, we display the analytical equations for all these correlations for Q_{ion}^{Max} with α, IE and N_v obtained through linear fit. These equations readily predict the peak of Q_{ion} for targets of similar size and structures.

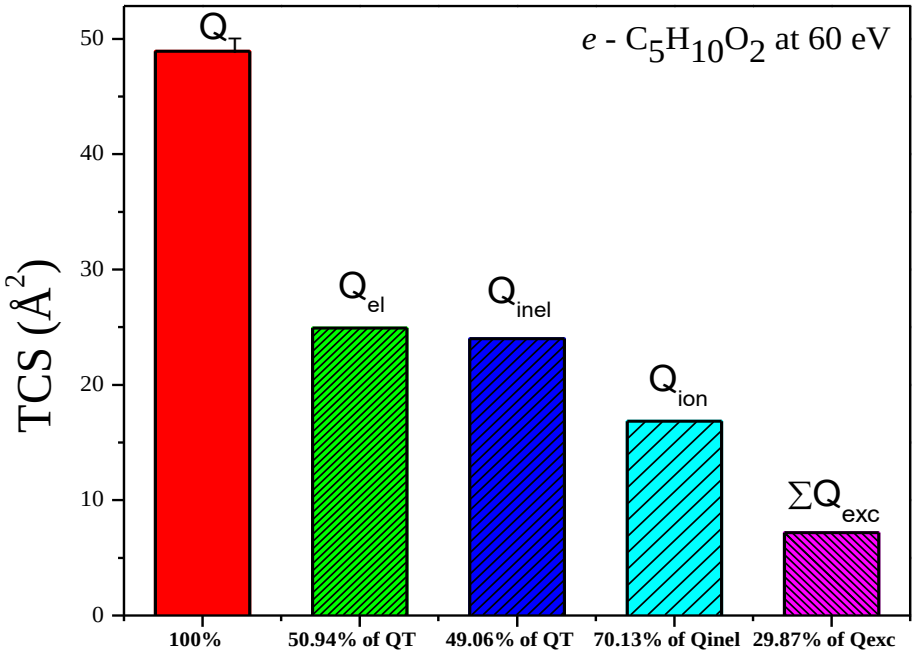

Figure 3.12 Relative cross sections

Figure 3.12 exhibits a variety of total CSs for e-$C_5H_{10}O_2$ scattering at 60 eV peak of Q_{inel} calculated through the quantum mechanical approach. Since Total CSs (Q_T) contain all scattering processes, they set the upper bound for all CSs. The elastic CSs (Q_{el}) is ~50.94% of Q_T and the inelastic (Q_{inel}) CSs is ~49.06% of Q_T. The contribution from the Q_{inel} and Q_{el} cross-sections is almost similar at the maxima of the Q_{inel} [29]. Due to the spherical approximation and GAR involved in present calculations the contribution of Q_{inel} to Q_T is not 50%. The contribution of the Q_{ion} is ~70.13% and Q_{exc} is ~29.87% of Q_{inel} is found as expected.

3.6 Chapter summary

In chapter 3 we reported our results on electron interaction (~10 eV - 5 keV) with biomolecular target: 3H-THF and THFA. For that we employed SCOP formalism along with CSP-ic formalism to compute Q_{el}, Q_T, Q_{inel}, $\sum Q_{exc}$, and Q_{ion} CSs data shown in (Figure 2 to 6). This is the first attempt to compute $\sum Q_{exc}$ for studied molecules in normal state. In this study we have found the following empirical correlations: (1) The Q_{ion} rises as the geometric structure and the number of electrons (N) of molecules increase. (2) Peak of Q_{ion} is significantly influenced by the target's ionization threshold. (3) present study has confirmed correlation between Q_{ion}^{Max}

and dipole polarizability (α) of present molecules, also Q_{ion}^{Max} linearly dependent with $\sqrt{\boldsymbol{\alpha/I_p}}$. (4) The results of this approach are in good accord with theoretical and experimental for the molecules discussed in this study. Present study enhances our confidence and also convinced for different methods that we have used to calculate CSs for present complex biological molecules with adequate speed and accuracy.

3.7 Bibliography

[1] A. D. Bass and L. Sanche, *Absolute and Effective Cross-Sections for Low-Energy Electron-Scattering Processes within Condensed Matter*, Radiation and Environmental Biophysics.

[2] H. Ibach and D. L. Mills, *Electron Energy Loss Spectroscopy and Surface Vibrations* (1982).

[3] D. Bouchiha, J. D. Gorfinkiel, L. G. Caron, and L. Sanche, *Low-Energy Electron Collisions with Tetrahydrofuran*, Journal of Physics B: Atomic, Molecular and Optical Physics **39**, 975 (2006).

[4] B. Boudaiffa, P. Cloutier, D. Hunting, M. A. Huels, and L. Sanche, *Resonant Formation of DNA Strand Breaks by Low-Energy (3 to 20 EV) Electrons.*, Science (1979) **287**, 1658 (2000).

[5] A. Kułakowski, *The Contribution of Marie Skłodowska-Curie to the Development of Modern Oncology*, Anal Bioanal Chem **400**, 1583 (2011).

[6] A. Muñoz, F. Blanco, G. Garcia, P. A. Thorn, M. J. Brunger, J. P. Sullivan, and S. J. Buckman, *Single Electron Tracks in Water Vapour for Energies below 100 EV*, Int J Mass Spectrom **277**, 175 (2008).

[7] Q. B. Lu and L. Sanche, *Effects of Cosmic Rays on Atmospheric Chlorofluorocarbon Dissociation and Ozone Depletion*, Phys Rev Lett **87**, 78501 (2001).

[8] R. I. Kaiser, *Experimental Investigation on the Formation of Carbon-Bearing Molecules in the Interstellar Medium via Neutral-Neutral Reactions*, Chem Rev **102**, 1309 (2002).

[9] M. G. Kong, G. Kroesen, G. Morfill, T. Nosenko, T. Shimizu, J. van Dijk, and J. L. Zimmermann, *Plasma Medicine: An Introductory Review*, New J Phys **11**, (2009).

[10] M. J. Eisenberg, J. Afilalo, P. R. Lawler, M. Abrahamowicz, H. Richard, and L. Pilote, *Cancer Risk Related to Low-Dose Ionizing Radiation from Cardiac Imaging in Patients after Acute Myocardial Infarction*, CMAJ **183**, 430 (2011).

[11] D. M. Sridharan, L. J. Chappell, M. K. Whalen, F. A. Cucinotta, and J. M. Pluth, *Defining the Biological Effectiveness of Components of High-LET Track Structure*, Radiat Res **184**, 105 (2015).

[12] D. W. O. Rogers, *Fifty Years of Monte Carlo Simulations for Medical Physics*, Physics in Medicine and Biology.

[13] C. Limbachiya, M. Vinodkumar, M. Swadia, K. N. Joshipura, and N. Mason, *Electron-Impact Total Cross Sections for Inelastic Processes for Furan, Tetrahydrofuran and 2,5-Dimethylfuran*, Mol Phys **113**, 55 (2015).

[14] P. Mozejko and L. Sanche, *Cross Sections for Electron Scattering from Selected Components of DNA and RNA*, Radiation Physics and Chemistry **73**, 77 (2005).

[15] A. R. Milosavljević, F. Blanco, J. B. Maljković, D. Šević, G. García, and B. P. Marinković, *Absolute Cross Sections for Elastic Electron Scattering from 3-Hydroxytetrahydrofuran*, New J Phys **10**, (2008).

[16] V. Vizcaino, J. Roberts, J. P. Sullivan, M. J. Brunger, S. J. Buckman, C. Winstead, and V. McKoy, *Elastic Electron Scattering from 3-Hydroxytetrahydrofuran: Experimental and Theoretical Studies*, New J Phys **10**, (2008).

[17] H. v. Duque et al., *Cross Sections for Electron Scattering from α-Tetrahydrofurfuryl Alcohol*, Chem Phys Lett **608**, 161 (2014).

[18] J. N. Bull, J. W. L. Lee, and C. Vallance, *Absolute Electron Total Ionization Cross-Sections: Molecular Analogues of DNA and RNA Nucleobase and Sugar Constituents*, Physical Chemistry Chemical Physics **16**, 10743 (2014).

[19] P. W. Stokes, S. P. Foster, M. J. E. Casey, D. G. Cocks, O. González-Magaña, J. de Urquijo, G. García, M. J. Brunger, and R. D. White, *An Improved Set of Electron-THFA Cross Sections Refined through a Neural Network-Based Analysis of Swarm Data*, (2021).

[20] A. R. Milosavljević, F. Blanco, D. Šević, G. García, and B. P. Marinković, *Elastic Scattering of Electrons from Tetrahydrofurfuryl Alcohol*, in *European Physical Journal D*, Vol. 40 (Springer New York, 2006), pp. 107–114.

[21] P. Mozejko, A. Domaracka, E. Ptasińska-Denga, and C. Szmytkowski, *Total Cross-Section Measurements for Electron Collisions with α-Tetrahydrofurfuryl Alcohol ($C_5H_{10}O_2$)*, Chem Phys Lett **429**, 378 (2006).

[22] A. Zecca, L. Chiari, G. García, F. Blanco, E. Trainotti, and M. J. Brunger, *Total Cross-Sections for Positron and Electron Scattering from α-Tetrahydrofurfuryl Alcohol*, New J Phys **13**, (2011).

[23] H. V. Duque et al., *Cross Sections for Electron Scattering from α-Tetrahydrofurfuryl Alcohol*, Chem Phys Lett **608**, 161 (2014).

[24] M. Vinodkumar, C. Limbachiya, M. Barot, M. Swadia, and A. Barot, *Electron Impact Total Ionization Cross Sections for All the Components of DNA and RNA Molecule*, Int J Mass Spectrom **339–340**, 16 (2013).

[25] C. Champion, *Quantum-Mechanical Predictions of Electron-Induced Ionization Cross Sections of DNA Components*, Journal of Chemical Physics **138**, 184306 (2013).

[26] P. W. Harland and C. Vallance, *Ionization Cross-Sections and Ionization Efficiency Curves from Polarizability Volumes and Ionization Potentials*, Int J Mass Spectrom Ion Process **171**, 173 (1997).

[27] M. Swadia, R. Bhavsar, Y. Thakar, M. Vinodkumar, and C. Limbachiya, *Electron-Driven Processes for Furan, Tetrahydrofuran and 2, 5-Dimethylfuran*, Mol Phys **115**, 2521 (2017).

[28] G. P. Karwasz, R. S. Brusa, A. Piazza, and A. Zecca, *Total Cross Sections for Electron Scattering on Chloromethanes: Formulation of the Additivity Rule*, Phys Rev A **59**, 1341 (1999).

[29] Joachain Charles, *Quantum Collision Theory (Amsterdam: North-Holland)* (1983).